Appl. Phys. A (2015) 121:765–771
DOI 10.1007/s00339-015-9478-4

Applied Physics A
Materials Science & Processing

Optical study of phase-separated thick InGaN layers grown on a compliant substrate

Jin-Ho Kang[1] · Mohamed Ebaid[1] · June Key Lee[2] · Sang-Wan Ryu[1,2]

Received: 19 April 2015 / Accepted: 4 September 2015 / Published online: 11 September 2015
© Springer-Verlag Berlin Heidelberg 2015

Abstract The optical properties of thick InGaN layers grown on a compliant substrate (CS) were investigated. The CS was fabricated by thermal deformation of nanoporous GaN during high-temperature annealing. The strain sharing between the InGaN with CS was characterized using high-resolution X-ray diffraction, and we found a reduced in-plane strain of the InGaN on the CS. Photoluminescence (PL) spectra exhibited double peaks associated with discontinuous strain relaxation during the growth of the InGaN films. The strain sharing suppressed defect formation in the InGaN grown on CS, whereas the degree of indium fluctuation was similar because the phase separation resulted from spinodal decomposition. The temperature dependence of the PL spectra and internal quantum efficiency were analyzed as a function of the thickness of the InGaN layer. The effects of the CS on the growth of thick InGaN layers are discussed.

1 Introduction

Group III nitrides, including AlN, GaN, InN, and their alloys, are promising materials for applications in solid-state lighting and high-power and high-speed electronics [1–3]. Moreover, considerable research effort has been invested in the development of group-III-nitride-based photovoltaic [4–6] and photoelectrochemical (PEC) devices [7, 8]. InGaN is particularly suitable for such applications because of the high charge carrier mobility and the control over the band gap, enabling devices operating at wavelengths from near-infrared (i.e., InN-based devices) to near-ultraviolet (i.e., GaN-based devices), which covers almost the entire solar spectrum. To realize InGaN-based photovoltaic or PEC devices, high-quality, thick layers of InGaN are required for optical absorption; however, the large lattice mismatch between InN and GaN makes it challenging to grow high-quality thick InGaN layers with a relatively high In content. The critical layer thickness (CLT) of an $In_xGa_{1-x}N$ layer with $x > 10\ \%$ is expected to be <100 nm based on the results of strain relaxation models [9] and gradually decreases with the increase in In content. Strain relaxation may occur when the thickness of the InGaN layer exceeds the CLT, which is accompanied by the formation of dislocations and often leads to compositional inhomogeneities and poor crystallinity [10–12].

Difficulties in growing InGaN layers on GaN substrates have led to the investigation of alternative lattice-matched substrates. ZnO is one of the most promising substrates for epitaxial growth of InGaN because of the crystalline symmetry and lattice matching to $In_{0.22}Ga_{0.78}N$ in the *a*-axis. Although ZnO may be expected to accommodate the formation of high-quality InGaN films, the high vapor pressure of Zn and the reactivity of ZnO with GaN lead to the formation of Ga_2ZnO_4 interfacial layers, which degrades the quality of the InGaN crystal layers [13–15]. New techniques, such as the use of GaN/InGaN superlattices and graded InGaN interlayers, have been proposed to address these issues [16]; however, the growth of high-quality InGaN layers remains an elusive goal.

The use of a compliant substrate (CS) has been proposed for lattice-mismatched epitaxy in order to release epilayer

✉ Sang-Wan Ryu
sangwan@chonnam.ac.kr

[1] Department of Physics, Chonnam National University, Gwangju 500-757, Republic of Korea

[2] Optoelectronics Convergence Research Center, Chonnam National University, Gwangju 500-757, Republic of Korea

strain [17–19]. Theoretical studies [20] have shown the possibility of heteroepitaxial growth of thick layers without degradation via strain sharing with the CS. Recently, thick SiGe layers have been grown on compliant silicon-on-insulator (SOI) substrates; these structures exhibited improved crystal quality compared with SiGe grown on a silicon substrate [17, 21]. Furthermore, locally freestanding Si nanomembranes have been used as a CS for the growth of InAs islands [22]. The growth of an InGaN layer on an appropriate CS, however, has not yet been reported.

In this work, we fabricated a thin CS via high-temperature deformation of nanoporous GaN. Thick InGaN layers were subsequently grown on the CS and were characterized and compared with those grown on a GaN/sapphire substrate (hereafter referred to as a reference substrate). The strain in the InGaN layer was shared with the CS, which increased the CLT of the InGaN. Thick InGaN layers on both the CS and the reference substrate were characterized optically using temperature-dependent photoluminescence (PL). We found double peaks in the PL spectra, which are related to the formation of lower and upper InGaN layers, each with different optical properties. Efficient optical emission from the InGaN layer grown on the CS was observed, which is attributed to the inhibition of defects due to reduced strain in the InGaN epilayer.

2 Experimental

The GaN layers used in this work were grown on *c*-plane sapphire substrates by metal organic chemical vapor deposition (MOCVD). The structure consisted of a low-temperature-grown GaN buffer, a 2-µm-thick unintentionally doped GaN layer, an 800-nm-thick highly doped *n*-type GaN layer (n^+-GaN, where $n = 8 \times 10^{18}$ cm^{-3}), and a 280-nm-thick *n*-type GaN layer (*n*-GaN, where $n = 4 \times 10^{18}$ cm^{-3}). Following the deposition of a 200-nm-thick SiO_2 layer using plasma-enhanced chemical vapor deposition, 3-µm-wide SiO_2 stripes were defined with a 3-µm separation on the *n*-GaN using conventional photolithography and wet etching, as shown in Fig. 1a. Electrochemical (EC) etching was then carried out using an EC cell with a Pt cathode, where the GaN sample was used as the anode [23]. The sample was immersed in 0.3-M oxalic acid, and etching was performed at room temperature. A constant voltage of 15 V was applied for 3 min to produce nanoporous (NP) layers of varying porosity in the n^+-GaN and *n*-GaN regions, as shown in Fig. 1b. The porosity of NP GaN was obtained from cross-sectional scanning electron microscope (SEM) image in which the proportion of pore region was evaluated. After removing the SiO_2 patterns using buffered oxide etchant and careful cleaning, the NP GaN sample was then reloaded into the MOCVD reactor for high-temperature annealing and growth of the InGaN layers. During the high-temperature annealing (at 1090 °C) in ambient hydrogen with ammonia, the highly porous layer was transformed into large voids, and the less porous layer was sealed via surface diffusion of atoms. This resulted in a thin GaN membrane, i.e., the CS, for the subsequent growth of a thick InGaN film. Because of the geometry of the NP layer, the CS was periodic in the plane of the wafer, being formed only between the SiO_2 stripes; hereafter we term this the patterned compliant substrate (PCS). $In_{0.11}Ga_{0.89}N$ layers that were 50, 100, and 150 nm thick were grown on the PCS at 770 °C under an ambient nitrogen environment, as shown in Fig. 1c. InGaN layers were grown on the PCS and on GaN/sapphire reference substrates and were characterized using X-ray diffraction (XRD) and temperature-dependent PL. Cathodoluminescence (CL) was utilized for spatially resolved images of InGaN layers.

3 Results and discussion

Figure 2a shows cross-sectional SEM images of the NP GaN formed by EC etching following the removal of the SiO_2 patterns. The etching morphology was controlled by varying the anodic voltage and the doping concentration. The low- and high-porosity layers were formed from the *n*-GaN and n^+-GaN layers, respectively, because the porosity was dependent on the doping concentration. The process of

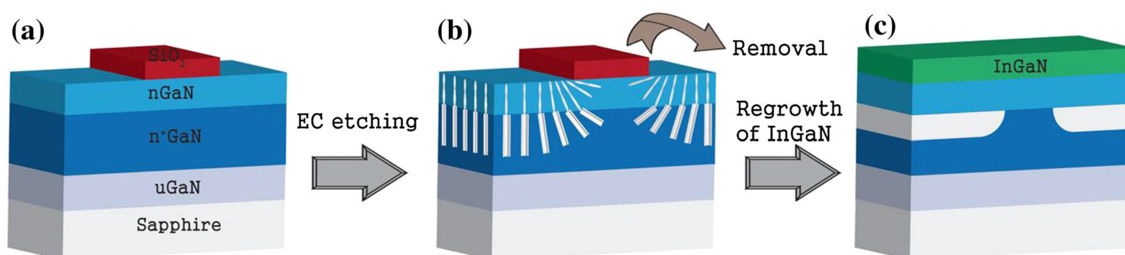

Fig. 1 Fabrication procedure of InGaN layers on the PCS. **a** Patterned SiO_2 on the *n*-GaN layer, **b** EC etching morphology of GaN layers with the patterned SiO_2, **c** fabrication of PCS by high-temperature annealing and growth of InGaN

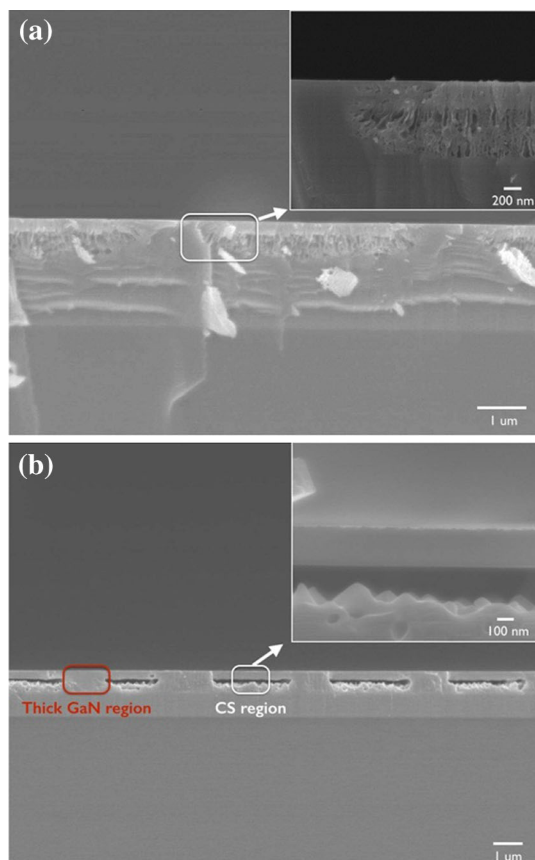

Fig. 2 Cross-sectional SEM images of **a** nanopores following EC etching and **b** the PCS following high-temperature annealing and the growth of a 50-nm-thick InGaN layer. The *insets* show magnified cross-sectional SEM images of the GaN membrane CS

forming NP GaN via EC etching and the resulting geometry around the patterned SiO_2 features has been reported previously [23]. The propagation of the NP etch deviated from vertical to horizontal because of the modification of the carrier depletion shape under reverse bias, which was caused by the electric field near the edge of the SiO_2 stripes. The measured porosity of the NP n-GaN layer was 10 % and that of the n^+-GaN was 65 %; however, the porosity varied continuously near the interface because of diffusion of the Si dopants during the growth of the n-GaN and n^+-GaN layers.

To fabricate the thin GaN membrane CS from the NP GaN layer, deformation of the NP GaN was accomplished via high-temperature annealing in ambient hydrogen with flowing ammonia to prevent decomposition of the GaN. Annealing was carried out at 1090 °C for 10 min, and a thick InGaN layer was then regrown at 770 °C. The transformation of the geometry of the NP GaN layers during the high-temperature annealing and regrowth has been reported previously [24, 25]. NP GaN is metastable at high temperatures because of the large surface area; this results in the transformation of the geometry of the nanopores via surface atomic diffusion. The highly porous layer was transformed into a layer containing spherical voids, and subsequently the voids in the GaN formed a porous network via the connection of neighboring voids following high-temperature annealing [23, 25]. The low-porosity layer was sealed due to surface diffusion; the thickness was slightly reduced to ~250 nm. This thin GaN membrane fabricated by thermal transformation would function as a CS for the heteroepitaxial growth of the InGaN layer. The PCS was composed of CS regions (67 % of the total area) surrounded by thick GaN regions, which provides stability to the CS membranes, as shown in Fig. 2b.

Figure 3 shows XRD ω–2θ measurements along the (0002) plane of the 50-nm-thick InGaN layers on the PCS and on the reference substrate. The molar fraction of In was ~11 % (i.e., the composition was $In_{0.11}Ga_{0.89}N$). The peak position of InGaN on the PCS was slightly shifted toward the GaN peak compared with that grown on the reference substrate. This shift can be explained by strain sharing between the InGaN layer and the GaN membrane [26, 27]. The InGaN epilayer grown on the CS exhibited a smaller lattice mismatch along c-axis than did that grown on the reference substrate. The in-plane strain can be expressed as

$$\varepsilon_m = (a_s - a_f)/a_f, \tag{1}$$

where a_s and a_f are the in-plane lattice constants of GaN and InGaN, respectively. The $In_{0.11}Ga_{0.89}N$ layer on the reference substrate had a large in-plane strain of $\varepsilon_m = -1.2$ %. The in-plane strain of the GaN/InGaN system can be relieved by sharing the strain in the InGaN layer ε_f, with that in the GaN layers ε_s. The strain in these two layers is modified according to [26, 27]

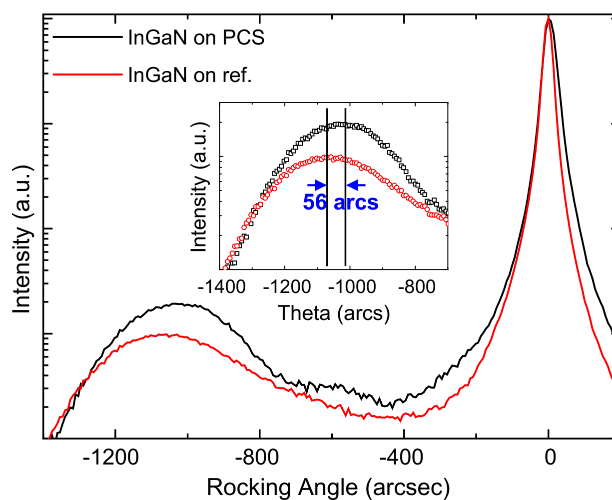

Fig. 3 High-resolution XRD data of the 50-nm-thick InGaN layers grown on the PCS and the reference substrate. The *inset* shows magnified view of InGaN peaks for the difference between the peaks

$$\varepsilon_f = \varepsilon_m h_s/(h_s + h_f) \quad \text{and} \quad \varepsilon_s = \varepsilon_m h_f/(h_s + h_f), \tag{2}$$

where h_f is the thicknesses of the InGaN layer, and h_s is the thickness of the GaN layer. InGaN grown on the PCS had less in-plane strain ($\varepsilon_m = -1.0$ %) than that grown on the reference substrate ($\varepsilon_m = -1.2$ %), and the c-axis lattice constant of the InGaN on the CS was smaller than that on the reference substrate, as determined from the shift in the peaks in the XRD rocking curve. The shift in the XRD peak of the InGaN layer grown on the CS region was 53 arcsec, which is close to the expected value calculated based on Eqs. (1) and (2) (i.e., 43 arcsec).

The effects of CS on the optical properties of 50-, 100-, and 150-nm-thick InGaN layers were investigated using temperature-dependent PL measurements. Figure 4a–c shows PL spectra of the InGaN layer grown on PCS, and Fig. 4d–f shows PL spectra for the InGaN layer grown on the reference substrate. For the 50-nm-thick InGaN layer, the PL spectra exhibited single emission peaks for both substrates. The full width at half maximum (FWHM) was 15.6 nm at 10 K for the InGaN layer grown on the PCS, which is relatively narrow compared with the PL emission peak on the reference substrate, where the FWHM was 37.6 nm. This suggests that the crystalline quality of the InGaN layer grown on the PCS was better than that of the InGaN grown on the reference substrate.

There exist a number of models to determine CLT of InGaN layers grown on GaN/sapphire substrates. The CLT differs somewhat depending on model used; however, the CLT of $In_{0.11}Ga_{0.89}N$ layers grown on GaN/sapphire substrates is in the range $10 < t_c < 100$ nm [9]. For an InGaN layer grown on a CS, the CLT can be expected to increase due to strain sharing between the InGaN layer and the CS. Several groups suggested that the effective CLT on a CS, t_{eff}, should be represented by [19, 28]:

$$1/t_{\mathrm{eff}} = 1/t_c - 1/t_s, \tag{3}$$

where t_c is the CLT on a GaN/sapphire substrate and t_s is the thickness of the CS. If the substrate is thinner than the CLT, then the effective CLT becomes infinite. In our experiments, the CS was relatively thick (~250 nm), which was larger than the thickness of the InGaN epilayer, which leads to only a modest increase in the CLT. For example, if $t_c = 50$ nm, we may expect $t_{\mathrm{eff}} = 63$ nm for InGaN grown on the 250-nm-thick CS. However, as shown in Fig. 4a, d, the increase in the CLT was sufficient to suppress or inhibit strain relaxation in the InGaN layer on CS, whereas significant strain relaxation occurred in the InGaN grown on the reference substrate, with the formation of dislocations and defects.

Periodic oscillations were observed in the emission spectrum of the InGaN grown on the reference substrate. This was attributed to interference effects due to multiple reflections of light at the air/InGaN and GaN/sapphire interfaces. However, PL from PCS sample did not exhibit these periodic interference fringes due to the thinner GaN membrane, which inhibited interference within the emission bandwidth of the PL.

The PL spectra exhibited double peaks when the thickness of the InGaN layer exceeded 50 nm. Dual peaks in the PL emission are well-known phenomena in thick InGaN and were characterized by several researchers, not only in bulk InGaN [10, 28, 29], but in InGaN quantum

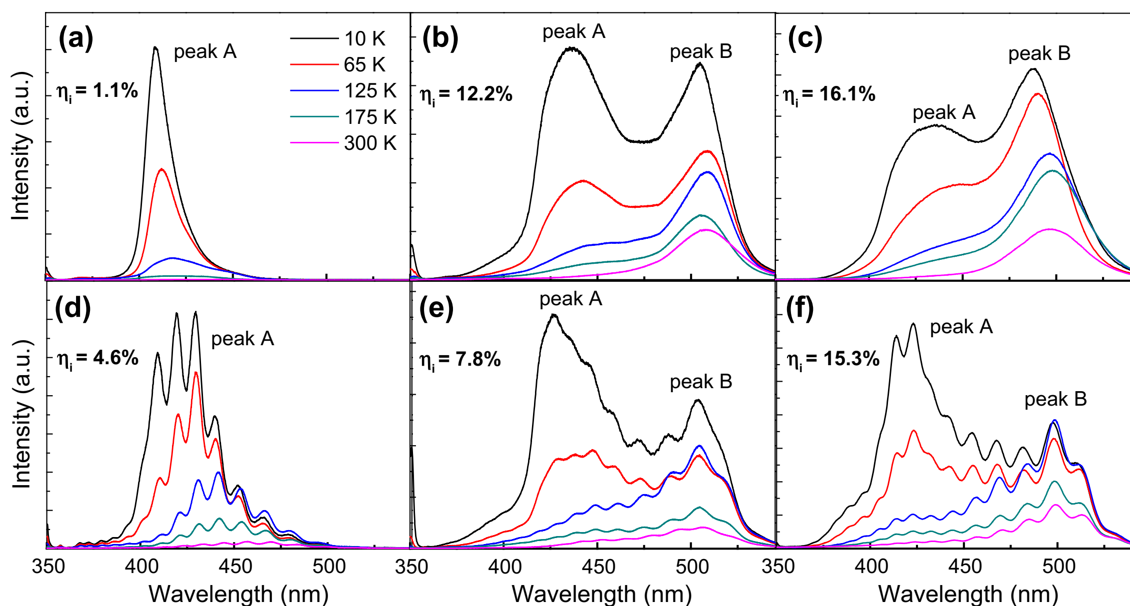

Fig. 4 Temperature-dependent PL of the **a**, **d** 50-, **b**, **e** 100-, and **c**, **f** 150-nm-thick InGaN layers on **a–c** the PCS and **d–f** the reference substrate

wells [30]. Such double peaks are attributed to the formation of double layers with distinctive optical properties during continuous growth of InGaN. These double layers are formed due to discontinuous strain relaxation, which leads to different wavelengths for PL emission [28]. The discontinuous strain relaxation was confirmed by Tsai et al. with XRD reciprocal space mapping [29].

The double peak in the PL emission due to InGaN on the PCS is shown in Fig. 4b, c. As the thickness of the InGaN layer increased from 100 to 150 nm, peak B grew in intensity, which indicates that this peak originated from the upper layer. Moreover, peak A was quenched at high temperatures, and peak B became dominant. Moon et al. [28] clarified the origins of both PL peaks by comparing PL spectra before and after removing the upper layer using reactive ion etching. They reported the disappearance of the longer-wavelength emission after removing the upper layer. Therefore, we may expect that the shorter-wavelength PL emission (peak A) originated from the lower InGaN layer and the longer-wavelength emission (peak B) from the upper layer.

The variation in strain relaxation is known to influence the In fluctuation [28, 31], although the fluctuations in the In content are primarily ascribed to spinodal decomposition of the InGaN layer due to thermodynamic instabilities. Using conventional approaches (i.e., growth on GaN/sapphire substrates), control over the strain in the InGaN layer should be accompanied by control over the In composition. The use of a CS, however, offers a method to separate the effects of strain and spinodal decomposition due to the In content, which makes a CS an interesting platform to investigate the effects of strain and In fluctuation on optical properties of thick InGaN layer.

The weak temperature dependence of peak B indicates that it originated from localized states, mostly related to variations in the In content of the upper layer. Phase separation due to fluctuations in the In content formed quantum-dot-like In-rich regions, and the modified density of states resulted in weaker temperature dependence of the PL emission. However, we believe that the fluctuations in the In content were suppressed in the lower layer because the growth of the epitaxial layer was strongly influenced by the substrate within the range of strain fields [32]. It follows that the energy for phase separation was modified, resulting in substrate-induced stabilization. This behavior is consistent with Ref [28] which reported the development of quantum-dot-like In-rich region only in upper InGaN layer.

The double-peak emission of the InGaN layer grown on the reference substrate (see Fig. 4e, f) exhibits different behavior compared with that grown on the PCS. As the thickness of the InGaN layer increased, the relative intensity of peak B decreased slightly, in contrast to the enhancement of peak B in the InGaN layer grown on the PCS. This was attributed to the formation of defects in the upper layer due to accumulated strain energy in the InGaN layer. We may therefore conclude that the thick InGaN layer grown on the PCS exhibited an increase in the intensity of peak B due to a reduction in the strain, whereas with the InGaN layer grown on the reference substrate, the intensity of peak B decreased by defect formation, though In fluctuation was observed similarly for both samples due to spinodal decomposition.

Figure 5 shows the integrated PL intensity as a function of temperature. We used the ratio of intensities $I_{\mathrm{PL(300K)}}/I_{\mathrm{PL(10K)}}$ as a measure of internal quantum efficiency η_i of the PL emission at room temperature. As all the samples showed constant PL intensity at low temperatures, the ratio could be a reliable approximation of η_i. We found that η_i increased as a function of the thickness of InGaN layer for both sets of samples, which is explained by carrier localization at the quantum-dot-like In-rich regions [10, 28]. It should be noted that 50-nm-thick InGaN layer on the PCS exhibited very low η_i despite the narrow emission bandwidth. We believe that this does not imply poor-quality epitaxial growth, but rather the onset of carrier escapes out of very thin InGaN layer. This effect is significant when the layer thickness is smaller than diffusion length and huge nonradiative centers are nearby. The roughened bottom

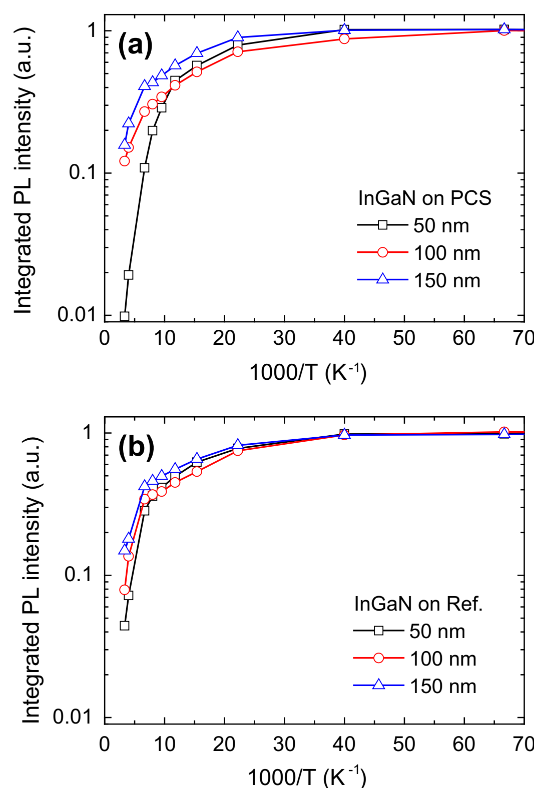

Fig. 5 Temperature dependence of integrated PL intensity of InGaN grown on **a** the PCS and **b** the reference substrate

surface of the GaN membrane that was formed during the fabrication of the PCS could be the nonradiative recombination sites. However, for the InGaN layers thicker than 50 nm, η_i was greatly improved due to the suppressed carrier diffusion by the formation of quantum-dot-like regions. Besides, η_i was larger for InGaN layers on PCS than on the reference. This is consistent with the PL emission spectra shown in Fig. 4, whereby the PCS inhibited the formation of defects and dislocations, so the 100- and 150-nm-thick InGaN layers exhibited larger η_i on the PCS than on the reference substrate despite the occurrence of surface recombination due to the thin membrane. It follows that the PCS enabled the growth of thick InGaN with improved optical properties while maintaining carrier localization.

Figure 6 shows CL measurements for 150-nm-thick InGaN on PCS at room temperature. Figure 6a displays the spatial mapping of emission intensity, which exhibited higher luminescence intensity at CS region. The enhanced emission intensity was attributed to improved crystallinity because of the compliancy of GaN membrane. The intensity fluctuation in CS region exhibited the existence of In fluctuation. CL spectra from both regions are shown in Fig. 6b. Both spectra were composed of two peaks, consistent with PL emission in Fig. 4. However, the long-wavelength peak (corresponding to peak B) was much enhanced on CS region. It was another evidence of the origin of peak B; it is from quantum-dot-like In-rich region formed by In fluctuation, and its high emission efficiency was attributed to the reduced defect density in CS region.

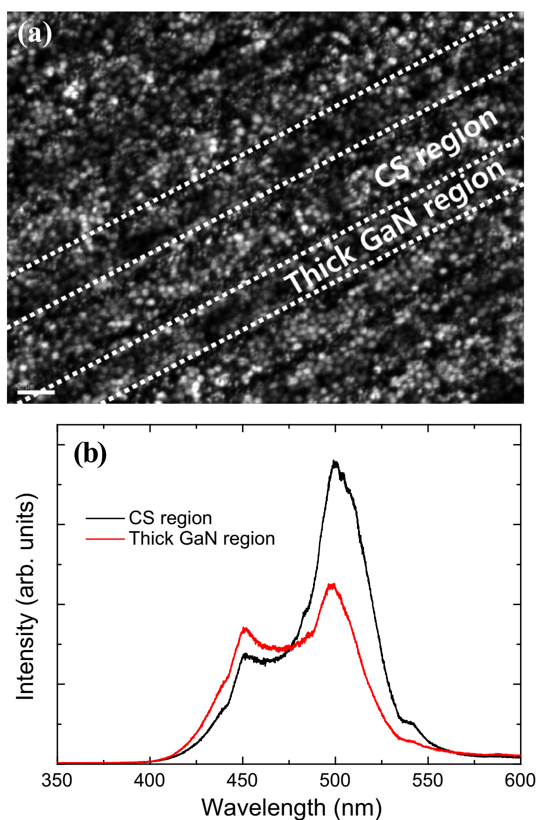

Fig. 6 **a** Spatial intensity mapping of CL emission from 150-nm-thick InGaN layer grown on PCS. Boundaries between CS regions and thick GaN regions were displayed by *dotted lines*. The *scale bar* represents 2 µm. **b** CL spectra from CS region and thick GaN region

4 Conclusion

The optical properties of thick InGaN epilayers grown on PCS were characterized using temperature-dependent PL. The PCS was formed of a 250-nm-thick GaN membrane that was fabricated using thermal deformation of nanopores during high-temperature annealing. Strain sharing with the compliant substrate was confirmed by reduced lattice mismatch along the *c*-axis for InGaN using high-resolution XRD. A narrow PL linewidth was obtained for the 50-nm-thick InGaN samples grown on the PCS, which provides evidence of the suppressed defect generation. Thicker InGaN films exhibited double PL peaks, which are associated with the formation of a double layer, with distinctive optical properties. In fluctuation due to phase separation was similarly observed for InGaN epilayers grown on the PCS and reference substrates; however, the optical properties differed depending on the substrate. For the longer-wavelength PL peak, the emission intensity was less sensitive to temperature due to the formation of quantum-dot-like In-rich regions; the peak due to this effect was more pronounced, with InGaN layers grown on the PCS, which is attributed to the suppression of defect generation owing to the compliance of the substrate.

Acknowledgments This work was supported by the National Research Foundation of Korea (NRF) Grant funded by the Korean Government (NRF-2013R1A1A2059179).

References

1. J.A. Alamo, J. Joh, Microelectron. Reliab. **49**, 1200 (2009)
2. E.F. Schubert, J.K. Kim, Science **308**, 1274 (2005)
3. Y. Li, J. Xiang, F. Qian, S. Gradcak, Y. Wu, H. Yan, D.A. Blom, C.M. Lieber, Nano Lett. **6**, 1468 (2006)
4. J. Wu, W. Walukiewicz, K.M. Yu, W. Shan, J.W. Ager III, J. Appl. Phys. **94**, 6477 (2003)
5. O. Jani, I. Ferguson, C. Honsberg, S. Kurtz, Appl. Phys. Lett. **91**, 132117 (2007)
6. R. Dahal, B. Pantha, J. Li, J.Y. Lin, H.X. Jiang, Appl. Phys. Lett. **94**, 063505 (2009)
7. A. Theuwis, K. Strubbe, L.M. Depestel, W.P. Gomes, J. Electrochem. Soc. **149**, E173 (2002)
8. X. Zheng, R.-H. Horng, D.-S. Wuu, M.-T. Chu, W.-Y. Liao, M.-H. Wu, R.-M. Lin, Y.-H. Lu, Appl. Phys. Lett. **93**, 261108 (2008)

9. S. Pereira, M.R. Correia, E. Pereira, C. Cowan, F. Sweeney, K.P. Donnell, E. Alves, N. Franco, A.D. Sequeira, Appl. Phys. Lett. **81**, 1207 (2002)
10. W.-C. Tsai, C.-H. Hsu, S.-F. Fu, F.-W. Lee, C.-Y. Chen, W.-C. Chou, W.-K. Chen, W.-H. Chang, Opt. Express **22**, A416 (2014)
11. A. Kar, D. Alexson, M. Dutta, M.A. Stroscio, J. Appl. Phys. **104**, 073502 (2008)
12. J. Adhikari, D.A. Kofke, J. Appl. Phys. **95**, 4500 (2004)
13. E.S. Hellman, D.N.E. Buchanan, D. Wiesmann, I. Brener, MRS Internet J. Nitride Semicond. Res. **1**, 16 (1996)
14. A. Kobayashi, H. Fujioka, J. Ohta, M. Oshima, Jpn. J. Appl. Phys. **43**, L53 (2004)
15. A. Kobayashi, J. Ohta, H. Fujioka, J. Appl. Phys. **99**, 123513 (2006)
16. S.-Y. Bae, Y.-H. Song, S.-R. Jeon, D.-M. Kim, Y.-D. Jho, D.-S. Lee, J. Cryst. Growth **387**, 23 (2014)
17. Z. Yang, J. Alperin, W.I. Wang, S.S. Iyer, T.S. Kuan, F. Semendy, J. Vac. Sci. Technol. **B16**, 1489 (1998)
18. A.M. Jones, J.L. Jewell, J.C. Mabon, E.E. Reuter, S.G. Bishop, S.D. Roh, J.J. Coleman, Appl. Phys. Lett. **74**, 1000 (1999)
19. Y.H. Lo, Appl. Phys. Lett. **59**, 2311 (1991)
20. D. Teng, Y.H. Lo, Appl. Phys. Lett. **62**, 43 (1993)
21. C.W. Pei, B. Turk, W.I. Wang, T.S. Kuan, J. Appl. Phys. **90**, 5959 (2001)
22. C. Deneke, A. Malachias, A. Rastelli, L. Merces, M. Huang, F. Cavallo, O.G. Schmidt, M.G. Lagally, ACS Nano **6**, 10287 (2012)
23. J.-H. Kang, M. Ebaid, J.K. Lee, T. Jeong, S.-W. Ryu, ACS Appl. Mater. Interfaces **6**, 8683 (2014)
24. C.D. Yerino, Y. Zhang, B. Leung, M.L. Lee, T.-C. Hsu, C.-K. Wang, W.-C. Peng, J. Han, Appl. Phys. Lett. **98**, 251910 (2011)
25. J.-H. Kang, J.K. Lee, S.-W. Ryu, J. Cryst. Growth **361**, 103 (2012)
26. J.P. Hirth, A.G. Evans, J. Appl. Phys. **60**, 2372 (1986)
27. J. Cao, D. Pavlidis, Y. Park, J. Singh, A. Eisenbach, J. Appl. Phys. **83**, 3829 (1998)
28. Y.-T. Moon, D.-J. Kim, J.-S. Park, J.-T. Oh, J.-M. Lee, Y.-W. Ok, H. Kim, S.-J. Park, Appl. Phys. Lett. **79**, 599 (2001)
29. S.M. Pereira, K.P. Donnell, E.J. Alves, Adv. Funct. Mater. **17**, 37 (2007)
30. J. Park, K.M. Song, S.-H. Moon, S.-W. Ryu, J. Electrochem. Soc. **157**, H739 (2010)
31. I.-K. Park, M.-K. Kwon, S.-H. Baek, Y.-W. Ok, T.-Y. Seong, S.-J. Park, Y.-S. Kim, Y.-T. Moon, D.-J. Kim, J. Appl. Phys. **87**, 061906 (2005)
32. S. Pereira, M.R. Correia, E. Pereira, K.P. O'Donnell, C. Trager-Cowan, F. Sweeney, E. Alves, Phys. Rev. B **64**, 205311 (2001)